



ELSEVIER

Available online at www.sciencedirect.com

SCIENCE @ DIRECT®

Palaeogeography, Palaeoclimatology, Palaeoecology 212 (2004) 23–44

PALAEO

www.elsevier.com/locate/palaeo

Evaluating climate change by multivariate statistical techniques on magnetic and chemical properties of marine sediments (Azores region)

Pieter A. Vlag, Pauline P. Kruiver, Mark J. Dekkers*

Paleomagnetic Laboratory 'Fort Hoofddijk', Department of Earth Sciences, Utrecht University, Budapestlaan 17, 3584 CD Utrecht, The Netherlands

Received 29 January 2003; received in revised form 28 May 2004; accepted 28 May 2004

Abstract

Regression models and cluster analyses are used to link magnetic properties of late Pleistocene deep-sea sediments in the Azores area (Mid-Atlantic Ocean) with the chemical element composition. The influence of the volcanic Azores Archipelago on sedimentation is evident in high magnetic mineral concentrations (low-field magnetic susceptibilities between 30 and 250×10^{-5} SI) and high Ti/Al ratios (>0.1). Variations in magnetic mineral concentration and Ti/Al ratios can be linked to detrital input and coincide with oxygen isotope ratio ($\delta^{18}\text{O}$) changes. The highest magnetic mineral concentrations and Ti/Al ratios are found around temperate climate periods, suggesting that detrital input from the Azores Islands is most prominent during these periods. Lower Ti/Al ratios and a slightly different composition of the lithogenic fraction suggests the presence of a second, probably eolian, detrital component during glacial periods. Higher Ba/Al ratios and 'excess Ba' estimates suggest higher productivity during the cold climate periods, especially at the end of stages 2 and 6. Temperate climate periods are characterised by a succession of peaks in magnetic mineral concentration and Ti/Al ratios at the beginning of these periods followed by peaks in CaCO_3 and Mn/Al toward the end. Cluster analysis shows that the first peaks might be related to volcanic material, which was initially deposited on land during eruptions in glacials and then washed into the sea due to the sea-level rise at the beginning of temperate periods. The latter peaks represent a more biogenic sediment signal, which might be more diagnostic of vegetation changes in the Azores Archipelago due to a warmer climate.

© 2004 Elsevier B.V. All rights reserved.

Keywords: Climate change; Multivariate statistical analysis; Magnetic properties; Chemical composition

1. Introduction

Numerous environmental studies have demonstrated that changes in properties of marine sediments may be linked to variations in detrital input, caused by

* Corresponding author. Tel.: +31 302531671; fax: +31 302531677.

E-mail address: dekkers@geo.uu.nl (M.J. Dekkers).

variations in aridity, wind strength and direction, fluvial input or ice-rafting (e.g. DeMenocal et al., 1993; Rea, 1994; Tiedemann et al., 1994). A complicating factor in environmental studies is that many magnetic and chemical parameters indicative of changes in detrital material are also influenced by post-depositional processes. Although the latter may be climate-dependent, it is crucial for the interpretation of climate records to separate the primary detrital from the secondary diagenetic signal. As a rule, a detrital magnetic signal can only be separated from diagenetic and biogenic signals by combining several magnetic parameters because individual parameters may have similar values. In practice, input source can only be traced with certainty when the magnetic signal is compared with other parameters, because the signal alters during erosion, transport and deposition of detrital particles. This has motivated recent work into combined magnetic and geochemical studies to detect environmental change (Rosenbaum et al., 1996; Vigliotti et al., 1999; Robinson et al., 2000; Larrasoña et al., 2003a). Here, we present a multidisciplinary environmental study, based on a combination of magnetic properties and element composition. The aim is to unravel detrital, diagenetic, and biogenic processes in marine sediments from the Azores Area for environmental reconstruction.

2. Geological setting

The marine sediments investigated are from core SU 92-18, a 9.9-m-long core collected from the Mid-Atlantic Ocean, close to the Azores Islands (37°47' 3 N, 27°13' 9 W). The water depth was 2300 m (Fig. 1), which is above the carbonate compensation depth during warm and cold climate periods. Its lithology is dominated by nannofossil ooze with clay minerals. The dominant clay minerals are smectite and illite. Several volcanic ash layers are intercalated in the sediments. A prominent tephra layer is situated between 5.82 and 6.05 m depth. Turbidite layers were detected neither visibly nor by magnetic anisotropy measurements (Kruiver et al., 1999), although the sediments were collected down-slope from the central islands of the Azores Archipelago.

Lehman et al. (1997) and Kruiver et al. (1999) studied these sediments to reconstruct the intensity of the ancient geomagnetic field. To obtain an age model, Lehman et al. (1997) measured a planktonic $\delta^{18}\text{O}$ record (Fig. 2) and correlated this record to the oxygen isotope curve of Martinson et al. (1987). Kruiver et al. (1999) correlated the $\delta^{18}\text{O}$ record from Lehman et al. (1997) with the SPECMAP curve. These authors observed a small offset between some magnetic and chemical parameters and the SPECMAP curve, there-

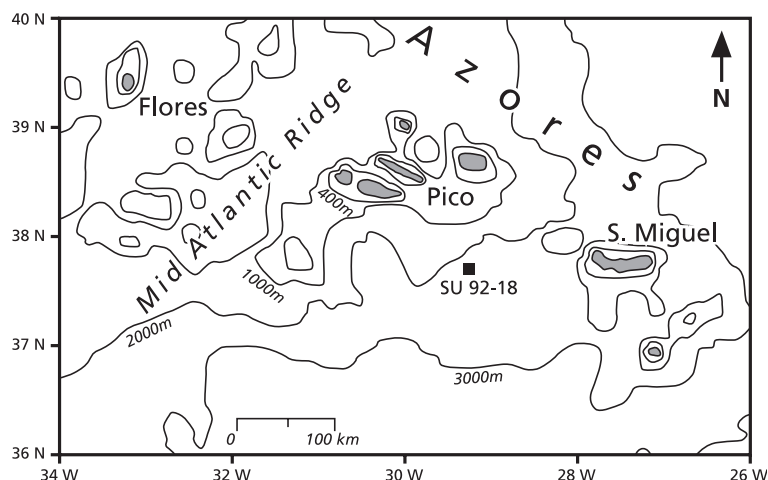


Fig. 1. Map of the Mid-Atlantic Ocean near the Azores Islands showing the location of core SU 92-18. Note that SU 92-18 is located down the southern slope from the Central Azores Islands.

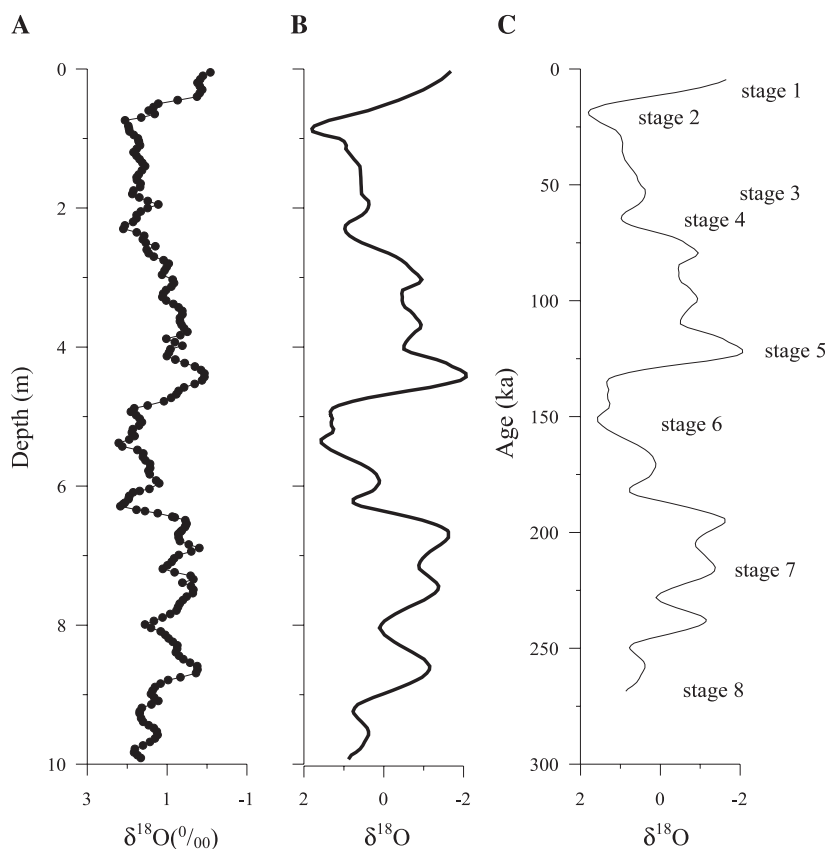


Fig. 2. (A) Measured oxygen isotope ratios of the planktonic foraminifer *Globigerina bulloides* from Lehman et al. (1997) and (B) their correlation with the SPECMAP curve. (C) SPECMAP $\delta^{18}\text{O}$ versus age.

fore the correlation of Kruiver et al. (1999) was re-examined for this study. This led to slight changes in the correlation between the measured $\delta^{18}\text{O}$ record and SPECMAP in the lowermost 2 m of the core, but left the interpretation for the uppermost 8 m unaffected (Fig. 2). All age-depth correlations show that the core covers the last 270 ky and has an average sedimentation rate of ~ 3.5 cm/ky.

Kruiver et al. (1999) measured various rock magnetic and chemical parameters to check whether the paleointensity record is affected by the environmental signal. This was shown not to be the case, although individual parameters showed climatic frequencies. The comparatively low measurement resolution did not permit conclusions to be made about relationships between magnetic, chemical, and climate records. Nonetheless, Kruiver et al. (1999) identified a number of intriguing aspects that warranted further

investigation. For this purpose, new magnetic and geochemical measurements were performed at a higher resolution. As we focus on the analysis of environmental change in the sediments, we have excluded the intercalated ash layers from interpretation. However, the same magnetic and geochemical information was gathered for the ash layers; they were considered as a compositional end member.

3. Methods

3.1. Magnetic mineralogy

Thermomagnetic runs and thermal demagnetization curves reveal that magnetite with a small amount of substituted Ti is the dominant magnetic mineral (Kruiver et al., 1999). No evidence for other magnetic

minerals was obtained with these measurements. Analysis of components of isothermal remanent magnetization (IRM) (Kruiver et al., 2001) enables the detection of minute amounts of magnetic minerals in the case of mixed magnetic mineralogy. Application of IRM component analysis to 15 samples from the present core only identifies the presence of low Ti-magnetite. This finding is crucial for the interpretation of the environmental magnetic signal. The presence of low Ti-magnetite over the entire core indicates a detrital magnetic signal for all climatic periods. The detection of only one magnetic mineral implies that variations in low-field magnetic susceptibility (χ), IRM and anhysteretic remanent magnetization (ARM) can be linked to changes in magnetic concentration and grain size.

3.2. Magnetic concentration and grain size

Cubic (8 cm³) specimens were used to measure χ , ARM and IRM. χ was measured for 204 specimens, taken at 4–5 cm intervals throughout the core. Its values range between 30 and 250 $\times 10^{-5}$ SI (Fig. 3). This is three orders of magnitude higher than the noise level of the instrument used (KLY-2 susceptibility bridge). ARM was imparted with an alternating field up to 125 mT superimposed on a bias field of 30 μ T. A PM4 pulse magnetizer was used to induce an IRM with a 1.5 T field. Both remanent magnetizations were measured with a JR5A spinner magnetometer. The ARM

intensities, measured on 170 samples, vary between 0.07 and 0.6 A/m (Fig. 3). IRM intensities measured on 95 samples are about a factor of 100 higher (Fig. 3). These intensities are high for sediments; 12 orders of magnitude above the noise limit of the JR-5A instrument. Values of χ , ARM, and IRM correspond to the reported values from Kruiver et al. (1999), indicating that the storage of the sediments at 4 °C between the Kruiver et al. (1999) study and the present one did not cause changes in magnetic properties.

Hysteresis loops were measured to obtain information about magnetic mineral concentration (M_s ; saturation magnetisation), magnetic grain size (M_r/M_s ; remanence ratio) and the relative concentration of dia- and paramagnetic minerals compared to the (ferri)magnetic signal (M_s/χ_{hf} : saturation magnetisation over high-field susceptibility). Loops were measured for 60 specimens (mass < 50 mg), equally spaced through the core, using an alternating gradient magnetometer (AGM) with a maximum field of 1 T. M_s ranges between 50 and 250 mAm²/kg (Fig. 4). M_r/M_s ranges between 0.2 and 0.3, indicating a pseudo-single domain state of the magnetic minerals (Fig. 4).

3.3. Elemental measurements

The elemental composition of the sediments was determined by X-ray fluorescence (XRF) measurements. Sediment samples were dried and ground and

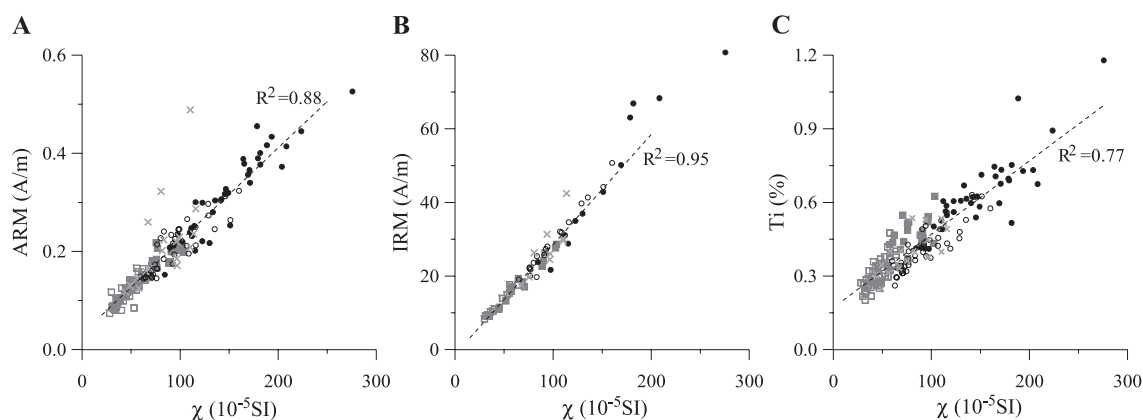


Fig. 3. Magnetic susceptibility (χ) versus (A) ARM intensity, (B) IRM intensity and (C) Ti content. Samples belonging to the ‘calcareous-low χ ’, ‘detrital-low χ ’, ‘calcareous-high χ ’ and ‘detrital-high χ ’ clusters (see description of the cluster model in Section 8 of the text) are represented by grey open squares, grey closed squares, black open circles and black closed circles, respectively. Grey crosses represent samples that were not assigned to a cluster (see text). Volcanic layers are not shown in this figure. The highest χ , ARM, IRM, and Ti values for the volcanic layers are 450 $\times 10^{-5}$ SI, 0.8 A/m, 120 A/m and 2.8%, respectively.

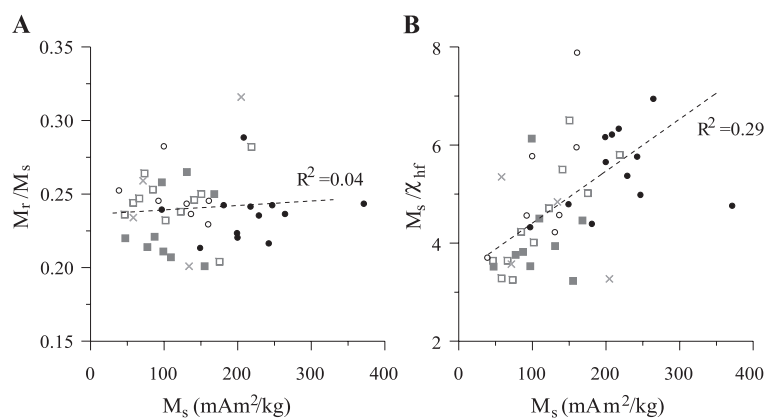


Fig. 4. Magnetic hysteresis measurements. (A) Remanence ratio (M_r/M_s) versus saturation magnetisation (M_s), (B) M_s divided by paramagnetic high-field susceptibility (M_s/χ_{hf}) versus M_s . Same symbols as in Fig. 3.

about 4.5 g of each powdered sample was mixed with 5.5 g pure quartz to obtain sufficient material for the measurements with a Bruker SRS3400 spectrometer. Precision and reproducibility were checked with laboratory standards and duplicate analyses. Analytical precision, checked by analysis of in-house standards, is better than 10%. Sample results can be reproduced with a variation smaller than 1%, making the reproducibility much better than the analytical precision. This implies that relative variations of elemental content within the core are precisely determined. The XRF analysis provided similar values as the ICPOES (inductively coupled plasma optical emission spectrometry) measurements from Kruiver et al. (1999), implying that absolute values of elemental concentrations (and ratios) are well determined.

Thirty five elements were analysed by XRF, but, for sake of clarity, the behaviour of only eight elements (Ti, Fe, Zr, Ca, Al, Ba, S, Mn) is discussed. These elements were selected because they are abundant and they provide useful discrimination among the detrital (Al, Ti, Fe, Zr), biogenic (Ca, Ba) and diagenetic (Fe, S, Mn) signals. Si is not considered further, because its reproducibility is slightly lower due to the correction for the quartz matrix. The most abundant element, Ca (15–35% of the element fraction per unit mass) is used to calculate the calcium carbonate (CaCO_3) content. CaCO_3 can be considered representative of the biogenic fraction, because the core is situated above the carbonate compensation depth. Al is representative of the lithogenic fraction and represents 1.5–6% of the element fraction by mass (Fig. 5). Al anti-correlates

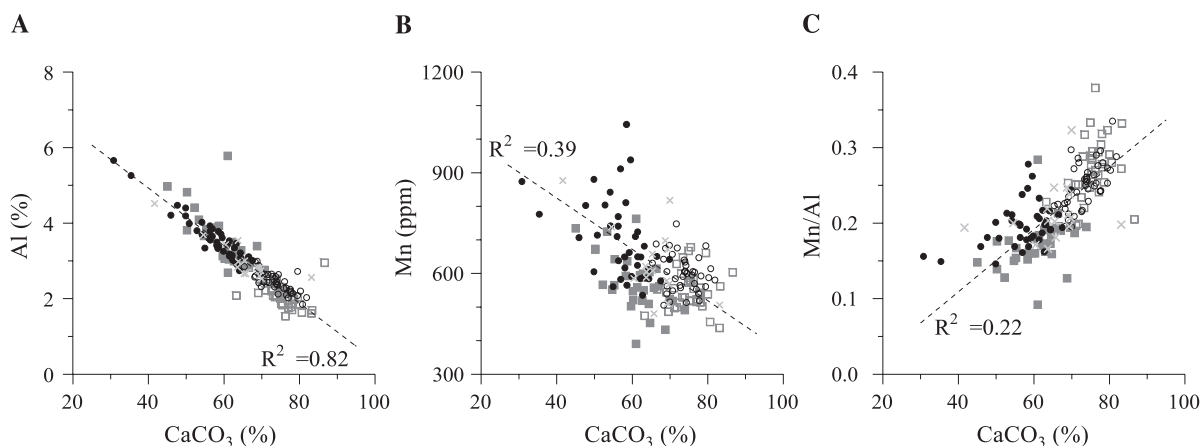


Fig. 5. Chemical element composition. (A) Al versus CaCO_3 , (B) Mn versus CaCO_3 and (C) Mn/Al versus CaCO_3 . Same symbols as in Fig. 3.

with CaCO_3 because the lithogenic and biogenic fractions together constitute the total sediment. To detect subtle changes in the chemical composition of the lithogenic sediment fraction, it is common to normalise chemical composition by Al.

4. Changes in individual parameters compared to the climate signal

4.1. The magnetic signal

With only one magnetic mineral detected, correlations between χ , IRM and ARM (Fig. 3) indicate that these three parameters dominantly reflect a magnetic concentration signal. Magnetic concentration pertains to a specific detrital signal because increasing M_s/χ_{hf} ratios with increasing M_s values (Fig. 4) show that magnetic concentration variations (M_s) are not accompanied by proportional variations in the paramagnetic clay matrix (χ_{hf}). M_r/M_s does not depend on magnetic mineral concentration (Fig. 4), but ARM/IRM decreases slightly with increasing χ (Fig. 6). The difference between these magnetic grain-size parameters may result from ARM/IRM being particularly sensitive to grain size changes just above the superparamagnetic-single domain threshold ($0.03 \mu\text{m}$ for magnetite) (Jackson, 1991; Tauxe et al., 1996), while M_r/M_s reflects grain-size variations of the average magnetic material. Therefore, an explanation may be that the relative concentration of fine grains relatively decreases with increasing magnetic concentration, but

that the bulk magnetic grain size is to a large extent independent of magnetic concentration variations.

The correlation between χ and Ti (Fig. 3) confirms that the magnetic mineral concentration reflects a detrital signal because Ti is a parameter for detrital input. In contrast to Ti, χ does not only depend on the amount of detrital input: it also depends on the presence of ultrafine superparamagnetic grains and paramagnetic minerals. This explains the variations in χ/Ti . The inverse correlation between χ/Ti and ARM/IRM (Fig. 6) excludes the possibility of a large effect of ultrafine superparamagnetic grains and paramagnetic minerals on the magnetic signal because χ/Ti ratios would then be independent of changes in ARM/IRM. Correlation between χ/Ti and ARM/IRM can, however, be easily explained by varying amounts of fine grains just above the superparamagnetic-single domain threshold size. These grains increase ARM/IRM, but reduce χ/Ti because just above the superparamagnetic-single domain threshold χ decreases with decreasing grain size.

4.2. Element geochemistry: changes in the lithogenic fraction

Normalizing Ti by Al reveals a striking relationship between Ti/Al and the $\delta^{18}\text{O}$ stratigraphy (Fig. 7). High Ti/Al ratios are observed around temperate climate periods, whereas lower ratios are found around cold climate periods. This indicates a strong correlation between detrital mineral input and climate. As Ti correlates with χ , it is not surprising that χ/Al

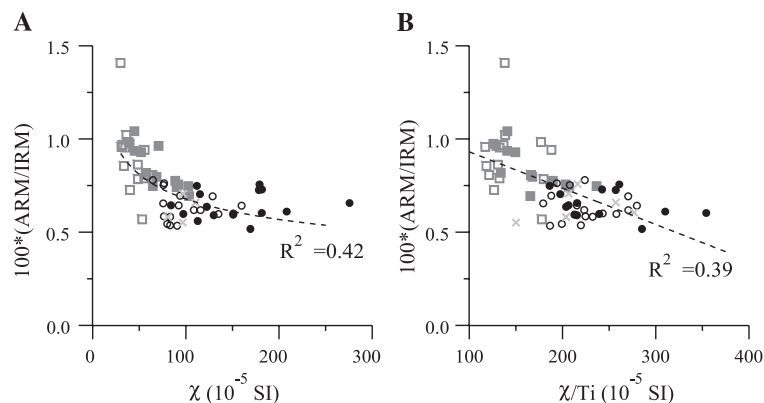


Fig. 6. (A) ARM/IRM versus χ , (B) ARM/IRM versus χ/Ti . Same symbols as in Fig. 3.

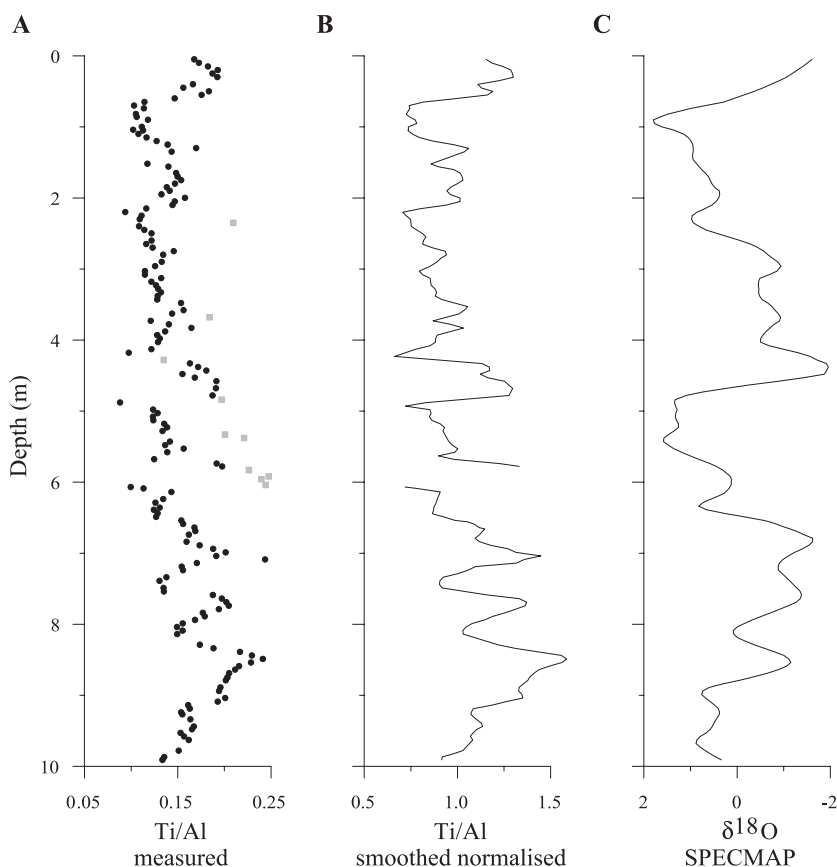


Fig. 7. (A,B) Changes in Ti/Al compared to (C) the standard SPECMAP $\delta^{18}\text{O}$ stratigraphy. Two depth profiles of the Ti/Al signal are shown; (A) raw data, (B) with a 20-cm-width triangular window smoothed data normalised with their median value. Black circles (grey squares) denote measured Ti/Al ratios of the sediments (volcanic ash layers). Volcanic ash layers are excluded for the calculation of the smoothed curves.

and χ also undergo similar variations as the $\delta^{18}\text{O}$ record (Fig. 8). Ti/Al shows a strong relationship with the $\delta^{18}\text{O}$ record, but the relationship between Zr/Al (Fig. 8), another proxy for detrital input, and $\delta^{18}\text{O}$ is complex. Typical of the Zr/Al depth profile are relatively thin stratigraphic intervals with extremely high Zr/Al ratios.

4.3. Element geochemistry: changes in the biogenic fraction

The use of Ba or Ba/Al ratios as a proxy for paleoproductivity is documented in many publications (see reviews by von Breymann et al., 1992; Wehausen and Brumsack, 1999). High Ba/Al ratios are found during cold climate periods, while lower Ba/Al ratios are observed during warm climate periods (Fig. 8). Ti/

Al shows the opposite relationship with the $\delta^{18}\text{O}$ stratigraphy: low Ti/Al ratios are observed in cold climate periods and high Ti/Al ratios are observed around temperate climate periods.

Barium dissolution may occur in organic-rich anoxic sediments (Brumsack and Gieskes, 1983; McManus et al., 1998). However, low sulphur concentrations ($\text{S} < 2000$ ppm) exclude anoxic conditions here. Furthermore, as soluble Mn^{2+} is mobilised in reducing environments and reprecipitated as oxyhydroxides under oxic conditions (Thomson et al., 1986), Mn enables detection of dissolution–precipitation cycles. If the Ba signal was affected by dissolution, minima in Ba would be expected around minima of Mn/Al. Such a relationship is not observed (Fig. 8). Hence, together with the low S content, Mn/Al indicates that changes in Ba/Al are not due to

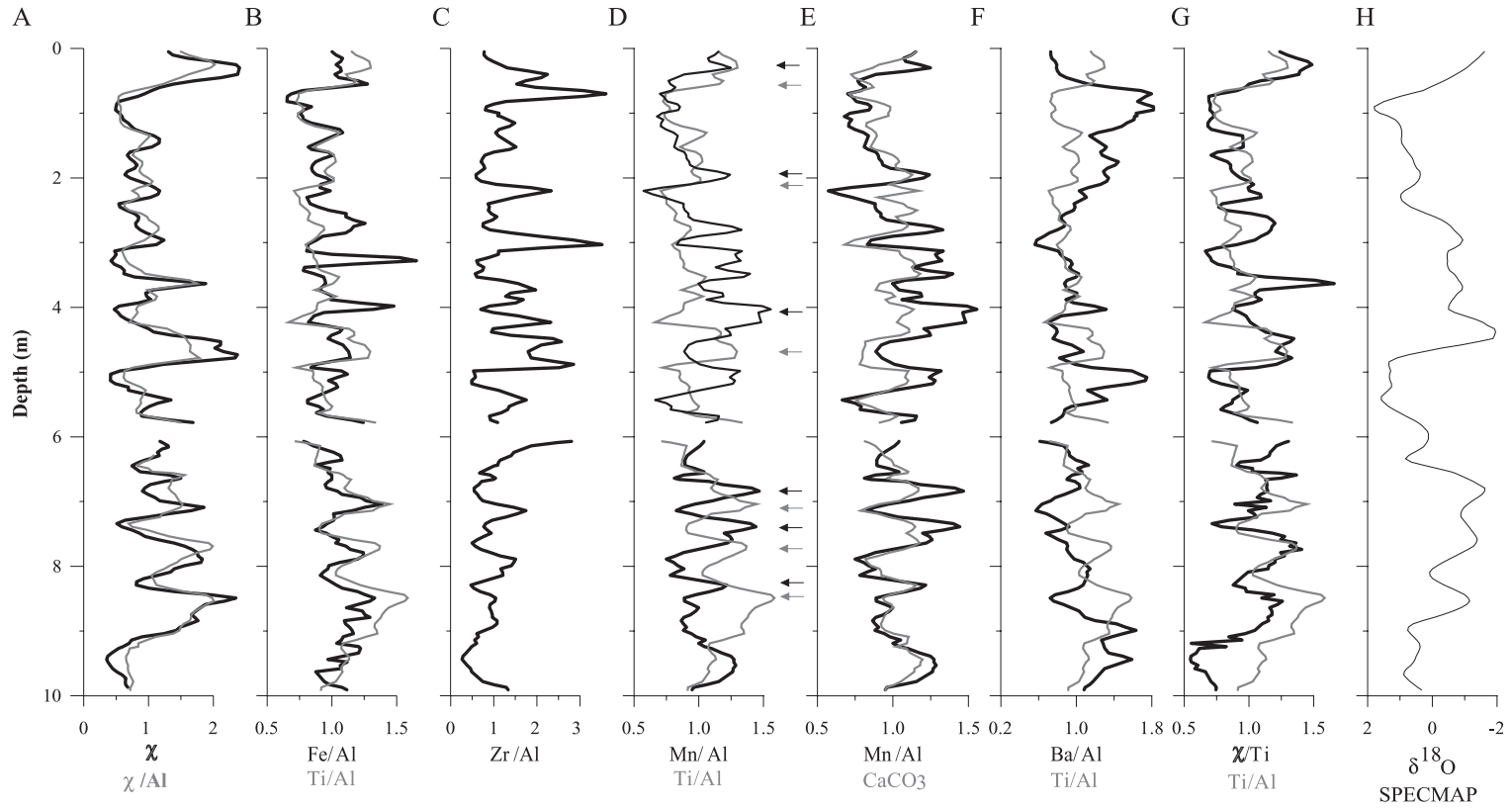


Fig. 8. Depth profiles for nine parameters (χ , χ/Al , Ti/Al , Fe/Al , Zr/Al , Mn/Al , CaCO_3 , Ba/Al , χ/Ti). Smoothed curves normalised by their median values (see Fig. 7) show the relationships between the down-core patterns of these parameters. Bold (grey) labels on the x-axis correspond with bold (grey) lines in the down-core plots. Ti/Al is shown as a reference parameter in several plots. This approach visualises an offset between peaks in Ti/Al and Mn/Al around temperate climate periods (see arrows). Mn/Al and CaCO_3 have similar trends except that changes around the temperate periods are more pronounced in Mn/Al than in CaCO_3 .

dissolution. This finding strongly suggests that Ba reflects a productivity signal in these sediments.

4.4. Element geochemistry: changes in the diagenetic fraction

Fe/Al has a similar signal to Ti/Al, indicating that these ratios reflect a detrital signal in most intervals. However, especially between 4 and 2 m depth, a few thin intervals with much higher Fe/Al ratios are observed (Fig. 8). Ti/Al does not show such abrupt changes, which suggests that dissolution–precipitation cycles affect Fe-content in these intervals.

If Mn is incorporated in CaCO₃, Mn should increase with increasing CaCO₃ content. This appears not to be the case. In contrast, samples with low CaCO₃ contents often have higher Mn concentrations (Fig. 5). Therefore, changes in Mn/Al can be related to diagenesis. Mn/Al correlates with the $\delta^{18}\text{O}$ stratigraphy, especially in the lower part of the core (depth 6–10 m; stages 7, 8) (Fig. 8). Like Ti/Al, Mn/Al ratios are higher around temperate climate periods. However, an offset between the Mn/Al and Ti/Al maxima is observed in these intervals. Maxima in Mn/Al typically occur 10–20 cm higher in the sediment column than maxima in Ti/Al (Fig. 8). This offset is two to four times larger than the sampling interval (5 cm) and is considered to be real.

5. Interpretation of the Ti/Al signal

Ti/Al ratios are used as a parameter for dust supply in the Eastern Mediterranean (Wehausen and Brumsack, 2000; Lourens et al., 2001; Larrasoña et al., 2003b). Eastern Mediterranean sediments are characterised by high Ti/Al ratios during cold climate periods and low Ti/Al ratios during warmer climate periods. An opposite relationship is found in this core: low Ti/Al ratios occurred during cold climate periods and high Ti/Al ratios occurred during warmer climate periods. Hence, the sedimentation model of the Mediterranean, a relatively more important fluvial input from the Nile River during temperate climate periods resulting in low Ti/Al ratios and an enhanced eolian input of Sahara dust during glacial periods resulting in high Ti/Al ratios, cannot be applied to the Azores area.

A major difference between the Azores area and the Eastern Mediterranean are the much higher Ti/Al ratios in the first region. The lowest Ti/Al ratios (~0.08) in the Azores core (Fig. 7) correspond to the highest Ti/Al ratios in the Eastern Mediterranean (Wehausen and Brumsack, 2000). Reported Ti/Al ratios from the northern Atlantic Ocean (Hinrichs et al., 2001) and Arabian Sea (Luckge et al., 2001) are also considerably lower than the Ti/Al ratios from this core. Of all rocks, volcanic rocks have the highest Ti/Al ratios. Generally, Ti/Al ratios for lavas are between 0.1 and 0.15 (e.g. Liotard et al., 1986; Lackschewitz and Wallrabe-Adams, 1997). Ashes from Iceland are reported to have even higher Ti/Al ratios: up to 0.2 (Lacasse et al., 1996; Lackschewitz and Wallrabe-Adams, 1997). The latter values are similar to the Ti/Al ratios measured for the intercalated ash layers (Table 2). Assuming that the Ti/Al ratios of the intercalated ash layers are typical of volcanic material from the Azores, the Ti/Al ratios of 0.1 up to 0.2 in core SU 92-18 (these high Ti/Al ratios were measured with both XRF and ICPOES analyses) can be explained by a mixture of this volcanic material with other detrital components characterised by lower Ti/Al ratios.

The land surface of the Azores islands is small (92 km²). Nevertheless, a comparatively large detrital input from these islands is possible because core SU 92-18 is situated down-slope of the Central Azores Island group (Fig. 1). The highest Ti/Al ratios are observed around temperate climate episodes, indicating that detrital input from the Azores Islands is most dominant in these intervals.

Lower Ti/Al ratios during the glacial periods show (larger) effects of other input source(s). Ice-rafted debris can be excluded because the core location is far beyond the southernmost limit of iceberg rafting (Bond et al., 1992). Taking into account the location of the studied site (in the Central Atlantic, far from continents) and a similar west–east surface circulation during temperate and cold climate periods, water transport is unlikely to have caused significant changes in detrital input. Our observations of larger effects of other detrital input sources during glacial periods fit well with the widely accepted idea that, due to a more vigorous atmospheric circulation, a weakened hydrological cycle, and extended dust source areas, average eolian deposition rates were considerably higher during glacial periods than during interglacial periods (e.g.

Rea, 1994; Mahowald et al., 1999). Taking into account that non-volcanic dust has lower Ti/Al ratios than volcanic ashes and rocks, the lower Ti/Al ratios may well result from more eolian deposition of Saharan dust. These findings based on Ti/Al ratios are of particular interest for this region; Mahowald et al. (1999) modelled global dust deposition during the Last Glacial Maximum (LGM) and their results suggest that the Azores Islands are situated on the edge of two zones. One toward the south and southeast with considerably higher dust deposition during glacials, caused by eolian transport of Saharan dust particles into the North Atlantic (e.g. Kolla et al., 1979; Moreno et al., 2001). The other one toward the north with similar dust deposition during glacials and interglacials.

6. Interpretation of the Ba/Al signal

In contrast to Ti/Al ratios the amplitude of the Ba/Al signal correlates with the amplitude of the climate variations as deduced from the $\delta^{18}\text{O}$ stratigraphy. The coldest periods of the studied time interval ($\delta^{18}\text{O}$ stages 2 and 6) correspond with the highest Ba/Al ratios (Fig. 8), while Ti/Al values in these intervals do not differ significantly from those observed in the short cold episodes during the temperate period of stage 7. Thus, both parameters show a different down-core pattern, although variations in both Ti/Al and Ba/Al are related to the $\delta^{18}\text{O}$ stratigraphy. Mathematically, this different pattern can be demonstrated by the poor significance of least-squares fits between Ba/Al and Ti/Al ($R^2 < 0.2$ with R^2 representing model variance over total variance). Similarly, least-squares fits reveal that Ba/Al hardly correlates with Fe/Al, Zr/Al, Mn/Al, CaCO_3 , Al, and χ . This indicates that Ba/Al is independent from detrital and diagenetic processes (Fig. 8).

A commonly used estimate for productivity is 'excess Ba', which is the Ba content corrected for detrital Ba background (Dymond et al., 1992):

$$\text{Ba}_{\text{excess}} = \text{Ba}_{\text{total}} - \text{Al}(\text{Ba}/\text{Al})_{\text{detrital}}$$

The detrital Ba background is unknown and has to be arbitrarily set. We used the mean of the 15 lowest Ba/Al ratios for this parameterisation. Although arbitrarily set, our estimate for the detrital Ba back-

ground is considered to be reasonable because the 15 lowest Ba/Al ratios correspond with temperate climate periods and in the present-day temperate climate period weak productivity is observed at this site. This choice yields estimates of $\text{Ba}_{\text{excess}}$ that are close to zero in temperate periods. $\text{Ba}_{\text{excess}}$ estimates are also negligible during the moderately cold climate period of stage 4 (Fig. 9). However, $\text{Ba}_{\text{excess}}$ is large during the glacials of stages 8, 6 and 2 (Fig. 9). This finding suggests that productivity was much stronger in these cold periods than during temperate climate periods.

Productivity in today's ocean is concentrated in margins characterised by coastal upwelling. A major zone of upwelling is concentrated off the coast of North Africa and the Iberian Peninsula (Sarnthein et al., 1988; Abrantes, 2000). Productivity was higher

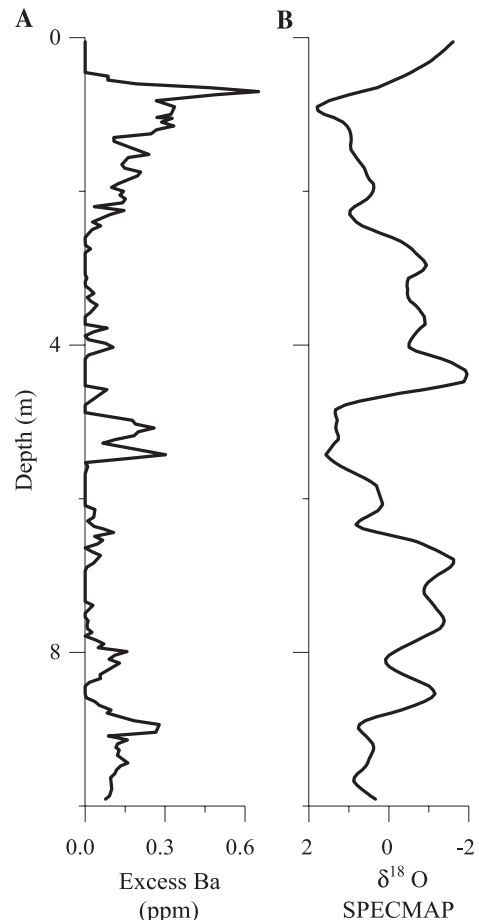


Fig. 9. (A) Excess barium versus depth compared with (B) the standard SPCCMAP $\delta^{18}\text{O}$ curve.

during the LGM than in the Holocene (e.g. Versteegh et al., 1996; Paillier and Bard, 2002). For the Iberian margin this is explained by intensification of the trade winds during cold climate periods, which strengthened the eastern boundary currents and upwelling off the eastern Atlantic (Abrantes, 2000; Paillier and Bard, 2002). The Azores Islands fall outside the upwelling zone off the Iberian Peninsula. However, they are situated at the same latitude and the interaction between the Canary Current and the trade winds is similar at this site and off the coast of the Iberian Peninsula. For this reason, it might be possible that the higher Ba/Al values during the glacials are due to small-scale upwelling on the west side of the Azores Archipelago during the LGM and older cold climate periods.

7. Linear regression models between element ratios

When x_i is perfectly measured and linearly correlated to y_i , variable x_i can be used to predict y_i with a simple linear regression model ($y_{\text{PREDICTED}, i} = \alpha + \beta_1 x_i$ with α and β calculated with the least squares method). Multiple regression models, where $y_{\text{PREDICTED}, i} = \alpha + \beta_1 x_{1i} + \beta_2 x_{2i} + \dots + \beta_p x_{pi} + \dots + r_i$, are useful if two conditions are fulfilled; (1) y_i depends on several factors represented by x_{1i}, \dots, x_{ni} and (2) the correlation coefficient R^2 of the least-squares fit between y and x_{1i}, \dots, x_{ni} is higher than the correlation coefficients of the fits between y and x_{1i}, \dots, x_{ni} separately. The last condition is fulfilled when the relationships between proxy y and the underlying factors are poor, but the underlying factors are mutually related.

Regression models are sensitive to outliers. To obtain outlier-robust regression models, a procedure proposed by Huber (1981) was applied. In a first step, an initial least-squares line is determined by using the original y -values. Then residuals r_i larger than a predetermined fixed cut-off c are bound to this cut-off value (smaller residuals remain unaffected). In a third step, y values are recalculated by adding the bounded residuals to the initially predicted y :

$$y_{i,\text{corrected}} = y_{\text{predicted}} + r_{i,\text{corrected}}.$$

Then, the corrected y values replace the original y -values and a new least-squares fit is calculated. This

procedure is repeated until no new residuals are bounded. The last fit in this iterative process is outlier-robust. Theoretically, the cut-off value depends on the distribution of the residuals (Huber, 1981). It is often cumbersome to determine this distribution. However, because outlier-robust regression models are not sensitive for slight changes in cut-off values, cut-off values are often arbitrarily set (Vlag et al., 2000). For this study, a residual r_i is bounded when its absolute value exceeds the threshold:

$$\begin{aligned} & 3\text{rd quartile } |r_i| + 1.5 * (3\text{rd quartile } |r_i| \\ & - 1\text{st quartile } |r_i|). \end{aligned}$$

7.1. Simple linear regression: detrital and diagenetic processes reflected by Fe/Al

Fe/Al versus Ti/Al plots show enhanced Fe/Al ratios for ~10% of the measured samples (Fig. 10). The enhanced ratios correspond with the Fe/Al peaks in the depth profiles (Fig. 8) and demonstrate the necessity for the use for outlier-robust linear regression models. The final outlier-robust fit between Fe/Al and Ti/Al differs substantially from the initial fit, but is a much better predictor for the remaining 90% of the samples as shown by a considerably higher R^2 (Table 1). As Fe/Al can be predicted with Ti/Al, a parameter for detrital input, it can be concluded that Fe/Al reflects a detrital signal, too.

The large positive residuals, measured Fe/Al ratios that are higher than predicted Fe/Al ratios, correspond with clear peaks in the Fe/Al down-core log. The added value of the regression model is that it demonstrates that these large residuals and thus implicitly peaks in Fe/Al do not depend on Ti/Al. As the peaks in Fe/Al are probably due to Fe-precipitation, this suggests that precipitation intervals are independent from the major detrital component in these sediments.

7.2. Simple linear regression: diagenesis, Mn/Al and Zr/Al

Major patterns of the Mn/Al depth profile can be predicted by an outlier-robust linear regression model between Mn/Al and Al (Fig. 11). The significance of this model is reasonable ($R^2=0.702$), despite the erratic pattern between Mn/Al residuals and Al (Table 1, Fig. 11). Positive residuals indicate that in warmer

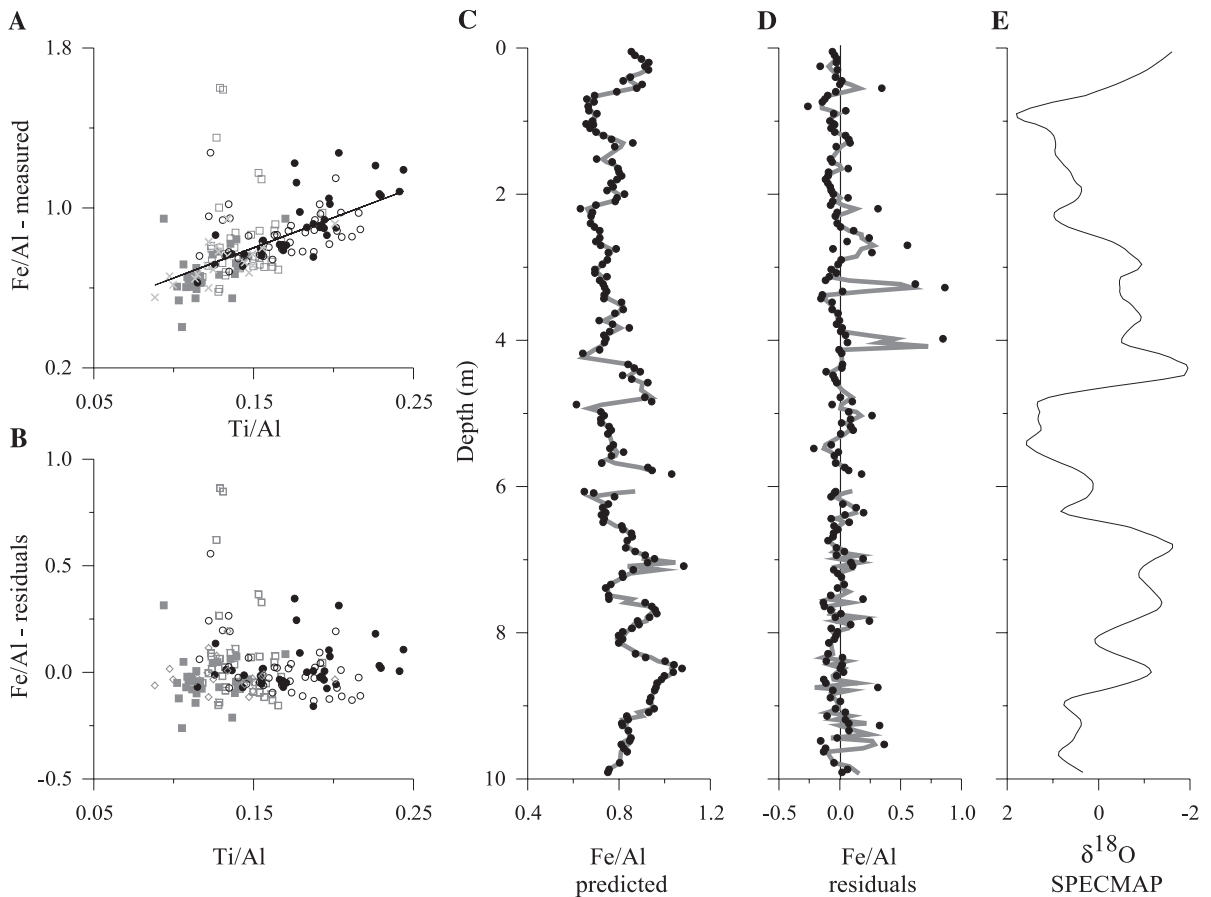


Fig. 10. (A) Fe/Al versus Ti/Al and the linear least squares fit between these parameters. The least squares line $\text{Fe/Al} = \alpha + \beta_1 \cdot \text{Ti/Al}$ is used to predict Fe/Al from Ti/Al (see text). (B) The validity of the model is demonstrated by homoscedastic residuals. (C,D) Predicted and residual Fe/Al plotted against depth. Peaks in residuals Fe/Al correspond with the peaks in Fe/Al, suggesting the occurrence of Fe-precipitation. In the x - y plots samples belonging to the 'calcareous-low χ ', 'detrital-low χ ', 'calcareous-high χ ' and 'detrital-low χ ' clusters are represented by grey open squares, grey closed squares, black open circles and black closed circles (as in Fig. 3). Grey crosses represent samples which could not be assigned to a cluster. Volcanic layers are not shown in this figure, because they are not included in the regression models.

periods the measured Mn/Al is generally higher than the predicted Mn/Al. This contrasts to colder periods, in which measured Mn/Al is generally lower than the predicted Mn/Al (Fig. 11). Hence, Mn/Al is influenced by two factors: (1) the lithogenic content in the sediments, as demonstrated by the fit between Mn and Al, and (2) a climate-dependant factor, as demonstrated by the residuals. The first factor has the largest effect on Mn/Al, because measured and predicted Mn/Al show similar trends and residuals are small (generally less than 10% of predicted Mn/Al). The origin of the second, climate-dependent, factor is unknown, but the results show that neither the

lithogenic fraction nor the Mn-signal are comparable between cold and warm climate periods.

An outlier-robust linear regression model to predict Zr/Al from Al shows similar results. The significance of this model is high ($R^2=0.817$, Table 1) and it predicts the major patterns of the Zr/Al depth profile (Fig. 12). However, clearly negative residuals show that predicted Zr/Al is too low in intervals corresponding to cold climate periods. This in contrast to warm periods, which show mostly positive or small negative residuals. Hence, like Mn/Al, two factors influence Zr/Al: (1) lithogenic content in the sediments, as demonstrated by the fit between Zr/Al and

Table 1
Results of simple and multiple linear regression models

Model	Robust	α	β_1	β_2	β_3	R^2
<i>Simple linear regression</i>						
(A) Fe/Al						
Fe/Al= α + β_1 Ti/Al	No	0.402	2,773			0.504
Fe/Al= α + β_1 Ti/Al	Yes	0.348	3,018			0.700
(B) Mn/Al						
Mn/Al= α + β_1 Al	No	0.369	-0.052			0.619
Mn/Al= α + β_1 Al	Yes	0.371	-0.053			0.702
(C) Zr/Al						
Zr/Al= α + β_1 Al	No	-0.053	-0.039			0.684
Zr/Al= α + β_1 Al	Yes	-0.038	-0.036			0.817
<i>Multiple linear regression</i>						
(D) χ						
χ = α + β_1 Al	No	117.4	350.8			0.372
χ = α + β_2 Ti/Al	No	-489.9		9107.0		0.417
χ = α + β_3 Ba/Al	No	1672.0			5752.9	0.262
χ = α + β_1 Al+ β_2 Ti/Al	No	-1571.3	361.6	9356.6		0.821
χ = α + β_1 Al+ β_2 Ti/Al+ β_3 Ba/Al	No	-1028.0	337.7	8379.6	-2412.9	0.863
χ = α + β_1 Al+ β_2 Ti/Al+ β_3 Ba/Al	Yes	-1027.6	335.7	8366.0	-2376.4	0.852

Regression coefficients α , β , and R^2 for initial (outliers not bounded) and robust (outliers bounded) least square fits. Robust models are used for the final prediction of Fe/Al, Mn/Al, Zr/Al and χ . χ is predicted with a multiple linear regression model. Coefficients of the linear least squares fits between χ and the predictors Al, Ti/Al and Ba/Al separately are also shown. R^2 is much lower for these separate fits than for the multiple linear regression model.

Al, and (2) an unknown climate-dependent factor, as demonstrated by the residuals.

The slightly different relationships between Zr/Al and Al and Mn/Al and Al for temperate and cold climate periods suggest subtle changes in the lithogenic fraction that is related to climate. As Zr/Al is indicative for the detrital fraction, these changes might be related to a detrital component. As usual, Al is used to correct for the amount of lithogenic fraction. It is conceivable that there are different provenance areas as function of climate. Ti/Al also indicates different sedimentation sources. If these would be characterised by somewhat different Al-content this could result in slightly different relationships between Zr/Al and Al and Mn/Al and Al for temperate and cold climate periods.

8. Prediction of χ from chemical elements with a multiple regression model

Due to a smaller effect of carbonate dilution, χ increases with increasing Al content (Fig. 13). Within the lithogenic fraction, changes in the detrital compo-

nent also affect the χ signal. This is demonstrated by the χ versus Al plot, which contains a sediment group with relatively high χ compared to Al and a sediment group with relatively low χ values, and the scattered χ -Ti/Al plot (Fig. 13). Therefore, significance levels of linear fits between χ and Al and between χ and Ti/Al are rather poor (Table 1).

The significance of the linear regression model for predicting χ with both Al and Ti/Al is high ($R^2=0.812$, Table 1). This can be explained by mutually related χ -Al and χ -Ti/Al relationships: samples with low χ values compared to Al also have low χ values compared to Ti/Al. As a result, Al and Ti/Al reinforce each other in the prediction of χ . This observation corresponds with the good correlations between χ and Ti (Fig. 3), because predicting χ by Al and Ti/Al ($\chi=\alpha+\beta_1$ Al+ β_2 Ti/Al) is a decomposition of predicting χ by Ti ($\chi=\alpha+\beta_1$ Ti). We chose this decomposition to separate the effects of dilution and detrital change on the χ signal.

Ba/Al has no direct link with χ because it reflects a productivity signal that is implicitly non-magnetic. However, neglecting this parameter in the regression model for the prediction of χ : $\chi=\alpha+\beta_1$.Al+ β_2 .Ti/Al

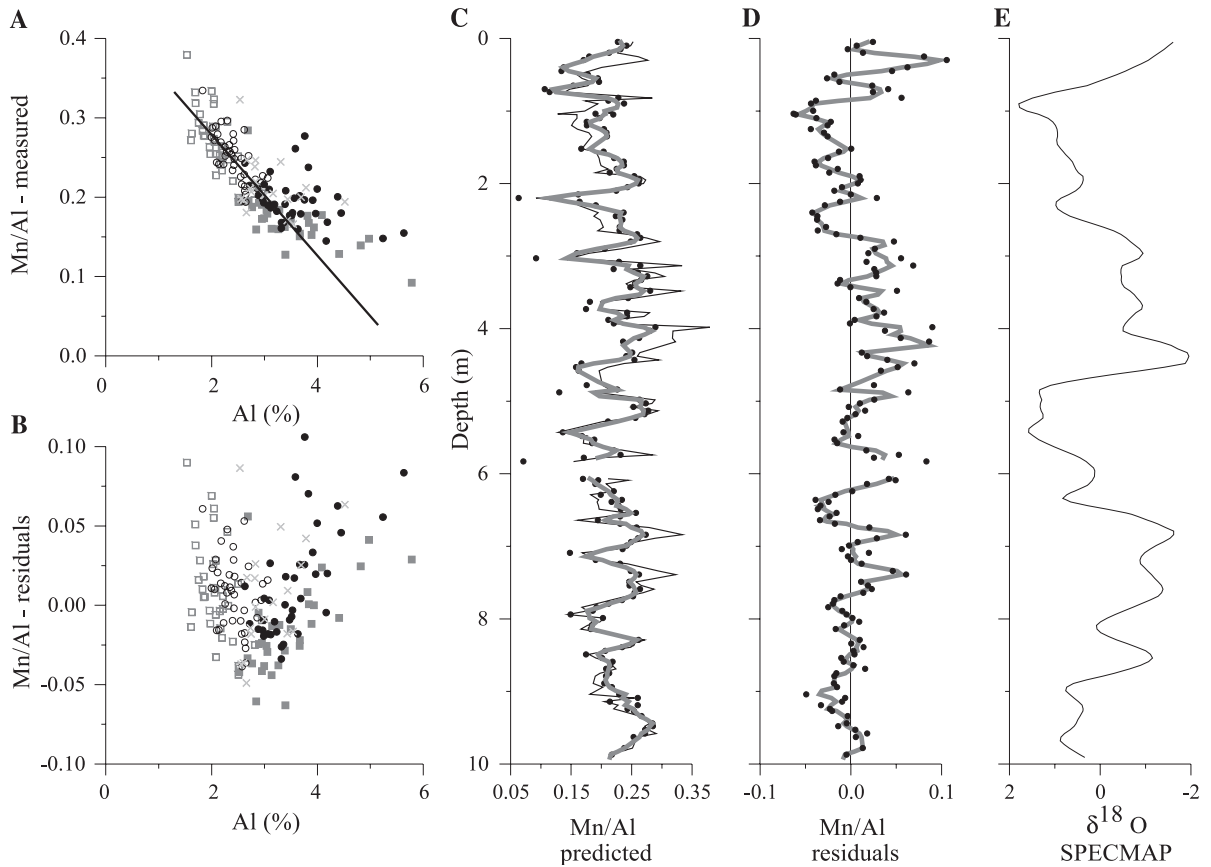


Fig. 11. (A) Mn/Al versus Al and the linear least squares fit between these parameters. The least squares line $Mn/Al = \alpha + \beta_1 Al$ is used to predict Mn/Al with Al. (B) Mn/Al residuals versus Al. (C) Predicted Mn/Al (black circles prediction per sample, grey line smoothed curve) and measured Mn/Al (thin line) plotted against depth. (D) Comparing the residuals (black circles residuals per sample, grey line smoothed curve) with (E) the standard SPECMAP $\delta^{18}O$ stratigraphy reveals that residuals tend to be negative during cold climate periods and positive during warm climate periods. Same symbols as in Fig. 10.

leads to overestimated χ 's in intervals with higher productivity (cold climate periods) and underestimated χ 's in intervals with low productivity (temperate climate periods) (Fig. 13). The influence of Ba/Al on the prediction of χ is also shown by slightly decreasing χ with increasing Ba/Al (Fig. 13). We attribute these observations to the dilution effect on χ by nutrients in periods of high productivity. Although related to nutrients and dilution, Ba and $CaCO_3$ reflect a different signal because no correlation exists between these parameters.

Like Al and Ti/Al separately, the linear correlation between Ba/Al and χ is poor ($R^2=0.262$, Table 1). However, adding Ba/Al to the multiple regression model improves the prediction of χ . First, the

significance of the model $\chi = \alpha + \beta_1 Al + \beta_2 Ti/Al + \beta_3 Ba/Al$ is higher than the significance of the model $\chi = \alpha + \beta_1 Al + \beta_2 Ti/Al$ (Table 1). Second, this model can be considered valid for all climate periods, because the residuals do not correlate with the $\delta^{18}O$ stratigraphy. The strongest point of this model is that it is easy to understand. $CaCO_3$ dilution explains the increasing χ with increasing lithogenic fraction. The strongly magnetic volcanic component within the lithogenic fraction explains the increasing χ with increasing Ti/Al ratios. The influence of Ba/Al on the susceptibility signal is probably caused by dilution. The significance of the model $\chi = \alpha + \beta_1 Al + \beta_2 Ti/Al + \beta_3 Ba/Al$ is high ($R^2=0.863$). This demonstrates that lithogenic fraction, detrital change,

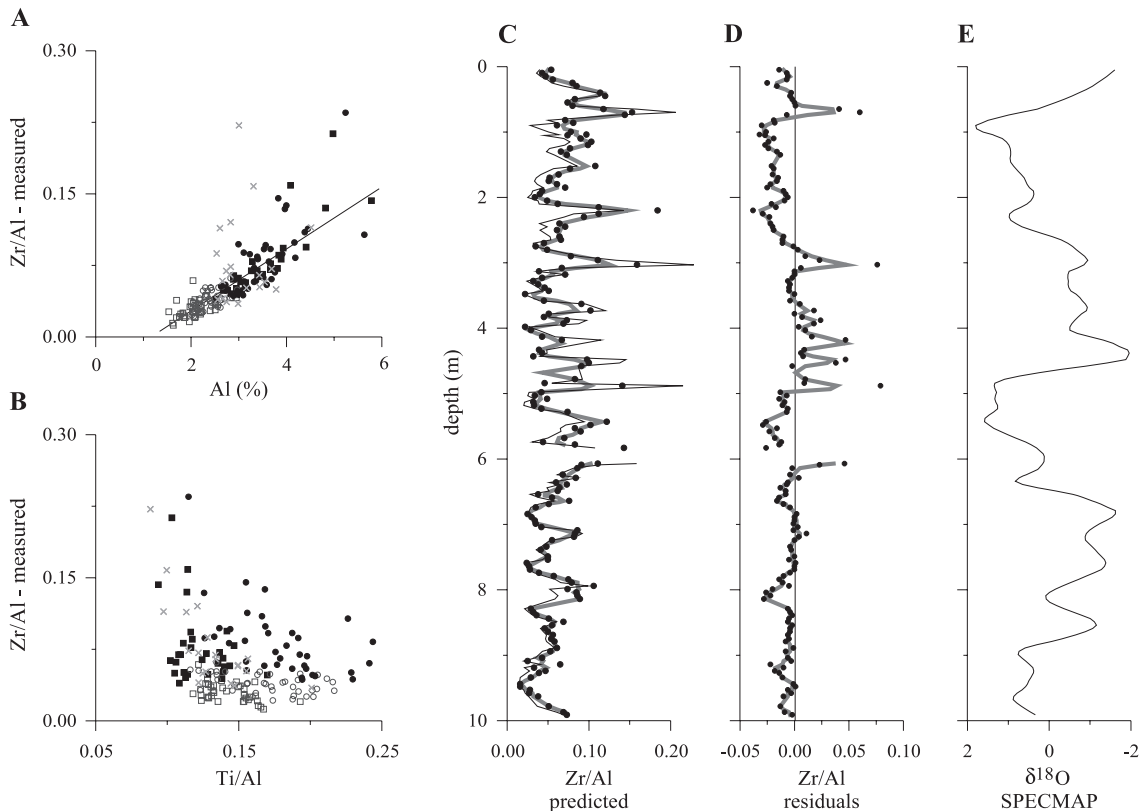


Fig. 12. (A) Zr/Al versus Al and the linear least squares fit between these parameters. The least squares line $Zr/Al = \alpha + \beta_1 \cdot Al$ is used to predict Zr/Al with Al. (B) The Zr/Al versus Ti/Al plot shows that no relationship between these parameters exist. (C) Predicted Zr/Al (black circles prediction per sample, grey line smoothed curve) and measured Zr/Al (thin line) plotted against depth. (D) Comparing the residuals (black circles prediction per sample, grey line smoothed curve with (E) the standard SPECMAP $\delta^{18}O$ stratigraphy reveals that residuals corresponding to a temperate climate tend to be higher. Same symbols as in Fig. 10.

and productivity explain the major features of the magnetic χ signal, and the effect of other factors on χ , like Fe-dissolution and precipitation and magnetic grain-size variations is limited in this Azores case study.

9. Fuzzy *c*-means clustering

Fuzzy *c*-means cluster analysis (Bezdek, 1981) is a partitioning method in which n cases are divided into a number of clusters to be specified by the user. The best clustering is calculated by minimising the distance between a sample (or case) and its cluster centre and maximising the distance between the cluster centres. The fuzzy concept implies that a sample is not forced to fit one cluster. Each sample

gets a membership to all clusters, which may range from 0 (no similarity between sample and cluster) to 1 (sample and cluster are identical). The memberships of each sample to all clusters add up to 1. A sample is assigned to a specific cluster if its highest membership exceeds a threshold to be specified by the user (in this study 50%). The fuzzy logic concept is attractive for sediment parameters because this concept is designed to treat gradually changing data. Vriend et al. (1988) and Dekkers et al. (1994) demonstrated the merit of fuzzy *c*-means clustering in combination with non-linear mapping (NLM) to isolate sample groups with similar geochemical and magnetic properties. This approach has been applied to several previous magnetic (Schmidt et al., 1999; Urbat et al., 1999) and combined magnetic-chemical studies (Urbat et al., 1999; Hanesch et al., 2001).

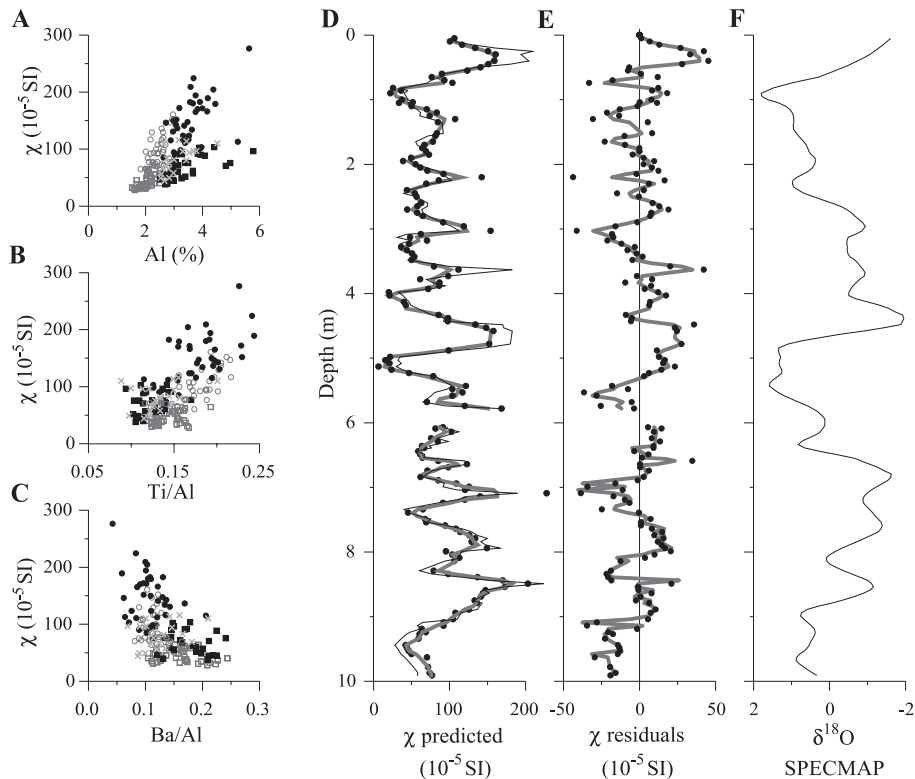


Fig. 13. Prediction of χ with the multiple regression model $\chi = \alpha + \beta_1 \text{Al} + \beta_2 \text{Ti/Al} + \beta_3 \text{Ba/Al}$. Three x - y plots show rather poor relationships between χ and (A) Al, (B) Ti/Al, and (C) Ba/Al. However, these three parameters together are a good predictor for χ , as shown by (D) similar depth profiles for predicted (thick grey line) and measured χ (thin black line). Predicted χ correlates with the standard SPECMAP $\delta^{18}\text{O}$ stratigraphy with higher values observed around temperate climate periods. (E) Residuals do not correlate with predicted χ showing that the model is homoscedastic. Neither do they correlate with (F) the standard SPECMAP $\delta^{18}\text{O}$ stratigraphy. Same symbols as in Fig. 10.

Cluster analysis depends on the relationships between the input variables and will be distorted if several input variables express the same phenomenon. Hence, an optimal interpretation of a cluster model is only possible if the relationships between the input variables are understood. For this reason, the variables for the cluster analysis (χ , M_r/M_s , M_s/χ_{hf} , CaCO_3 , Ti/Al, Zr/Al, Fe/Al, Ba/Al, Mn/Al and χ/Ti) were carefully selected. All parameters were logarithmically transformed before applying the fuzzy cluster algorithm, element/Al ratios were chosen to ascertain that the cluster composition can be related to the relationships between the underlying parameters (Aitchinson, 1984). ARM and IRM intensities, ARM/IRM and Al element abundance are not included in the cluster models because these parameters reflect a similar signal as χ , χ/Ti and CaCO_3 , respectively (Figs 3, 4 and 6).

Models containing five or more clusters appeared not to be robust: the results cannot be reproduced when a few randomly selected samples are excluded from the data set. The most detailed robust model, a four-cluster model, consists of: (1) a cluster with a high CaCO_3 content and low susceptibilities, (2) a cluster with high CaCO_3 contents and high susceptibilities, (3) a cluster with low CaCO_3 contents and low susceptibilities, and (4) a cluster with low CaCO_3 contents and high susceptibilities (Table 2). These four clusters are called 'calcareous-low χ ', 'calcareous-high χ ', 'detrital-low χ ' and 'detrital-high χ '. The term detrital is used for clusters with relatively low CaCO_3 because they are more lithogenic, and, especially for the cluster with the low CaCO_3 content and high susceptibilities, their properties are more similar to those of the volcanic ash layers (Table 2). 180 samples could be assigned to one of these four clusters

Table 2
Properties of the four clusters compared to the volcanic ash layers

	Cluster calcareous-low χ			Cluster detrital-low χ			Cluster calcareous-high χ			Cluster detrital-high χ			Volcanic layers		
	1st Quartile	Median	3rd Quartile	1st Quartile	Median	3rd Quartile	1st Quartile	Median	3rd Quartile	1st Quartile	Median	3rd Quartile	1st Quartile	Median	3rd Quartile
<i>Proxies included in cluster model</i>															
χ , $\times 10^{-5}$ SI	35.2	42.7	52.4	56.1	69.3	79.3	75.8	92.1	107.8	122.3	148.5	181.8	166.6	256.5	435.5
M_T/M_s	0.23	0.24	0.25	0.21	0.22	0.25	0.24	0.25	0.26	0.22	0.24	0.24	0.23	0.23	0.24
M_s/χ_{hf} , 10^6 A/m	3.37	3.83	4.71	3.45	3.79	4.03	4.38	4.56	6.82	4.81	5.50	6.18	5.28	5.57	5.76
CaCO ₃ , %	72.7	75.5	78.1	55.1	61.7	65.0	70.4	74.1	77.0	55.0	58.5	62.6	32.8	48.3	62.4
Ti/Al	0.13	0.14	0.16	0.11	0.12	0.14	0.15	0.17	0.19	0.16	0.18	0.20	0.19	0.22	0.24
Fe/Al	0.71	0.79	0.89	0.61	0.66	0.72	0.79	0.86	0.95	0.80	0.88	1.03	0.90	1.11	1.14
Zr/Al	0.02	0.03	0.04	0.05	0.07	0.08	0.03	0.04	0.05	0.06	0.08	0.10	0.08	0.09	0.14
Ba/Al	0.14	0.17	0.19	0.15	0.17	0.20	0.10	0.11	0.12	0.09	0.11	0.13	0.04	0.07	0.10
Mn/Al	0.24	0.27	0.29	0.15	0.17	0.18	0.23	0.25	0.28	0.18	0.19	0.20	0.16	0.17	0.19
χ/Ti , $\times 10^{-3}$ SI	126.8	138.5	169.0	138.7	162.3	191.5	212.8	224.8	244.8	213.0	233.1	258.1	205.8	222.1	336.7
<i>Proxies excluded for cluster model</i>															
Al, %	1.9	2.1	2.2	3.0	3.3	3.9	2.2	2.4	2.6	3.2	3.5	3.9	2.8	4.5	5.3
χ/Al , $\times 10^{-3}$ SI	2.6	3.7	4.6	3.6	5.0	6.1	6.1	6.8	8.9	6.1	7.7	9.7	4.6	6.2	8.4
ARM/IRM, $\times 100$	0.79	0.86	0.97	0.75	0.80	0.95	0.58	0.61	0.69	0.59	0.64	0.72	0.71	1.53	4.29

Cluster properties expressed by distribution parameters 1st quartile, median and 3rd quartile. These parameters are calculated by sorting the measured values x within a cluster in ascending order ($x_{(1)} < x_{(2)} < x_{(3)} < \dots < x_{(n)}$) before calculating the thresholds at which 25%, 50% and 75% of the sorted values are smaller, respectively. The parameters 1st quartile, median and 3rd quartile are outlier robust.

(Fig. 14). As most input parameters are related to climate, the four clusters are not randomly distributed throughout the core but are confined to specific intervals (Fig. 14). The 16 intermediate samples, which could not be assigned to a cluster, are mostly located at the boundaries of these intervals.

Links between magnetic mineral concentration, magnetic grain size, detrital input, and productivity explain the major differences between the two ‘low χ ’ and two ‘high χ ’ clusters (Table 2). The ‘low χ ’ clusters have considerably higher Ba/Al and ARM/IRM values, while χ /Ti, M_s/χ_{hf} , Ti/Al and Fe/Al

ratios are considerably higher in the ‘high χ ’ clusters. Linear correlations between Mn/Al, Zr/Al and the lithogenic fraction (Figs. 11, 12) explain the higher Mn/Al ratios and lower Zr/Al ratios in the calcareous clusters compared to detrital clusters (Table 2). Dilution effects on the susceptibility signal can be excluded when interpreting the cluster model, because cluster properties show similar trends to χ and χ /Al (Table 2).

The ‘detrital-high χ ’ and ‘calcareous-low χ ’ clusters are the end members in the four-cluster model. Comparison of median values of all parameters from the sediment clusters with the volcanic ash layers shows that the ‘detrital-high χ ’ cluster is most similar to the volcanic ash layers (Table 2). This suggests that the effect of detrital input from the nearby Azores Islands is the strongest for sediments belonging to this cluster. Evidently, the influence of volcanic ashes is smallest on sediment samples assigned to the ‘calcareous-low χ ’ cluster. This cluster is concentrated in three stratigraphic intervals. (1) The lowermost part of the core, corresponding to the glacial period of stage 8. (2) The coldest episodes of stages 6 and 2, which are intervals at which peaks in Zr/Al suggest a different detrital input. (3) The peaks in Fe/Al between 2 and 4 m depth, which are the only intervals where strong evidence for diagenesis is provided. Taking into account these observations, end member cluster ‘calcareous-low χ ’ is considered as heterogeneous: the effects of diagenesis on sediment properties cannot be neglected and possible effects of a deviating detrital input source seem to be the largest.

Higher Ti/Al, χ /Al, and χ values, and lower Ba/Al values are observed around temperate climate periods (Fig. 8). Matching this observation with the cluster properties explains that the two ‘high χ ’ clusters are found around temperate climate periods and the two ‘low χ ’ clusters in sediments deposited during cold climate periods (Fig. 14). An offset between maxima in Ti/Al and Mn/Al around the temperate periods (Fig. 8) explains a succession of ‘detrital-high χ ’ and ‘calcareous-high χ ’ clusters around the temperate climate periods. Comparison with the $\delta^{18}\text{O}$ stratigraphy confirms that ‘detrital-high χ ’ clusters tend to lie at the beginning of warm climate episodes (Fig. 14). They are followed by a ‘calcareous-high χ ’ cluster, which tends to be situated towards the end of the warm climate episodes.

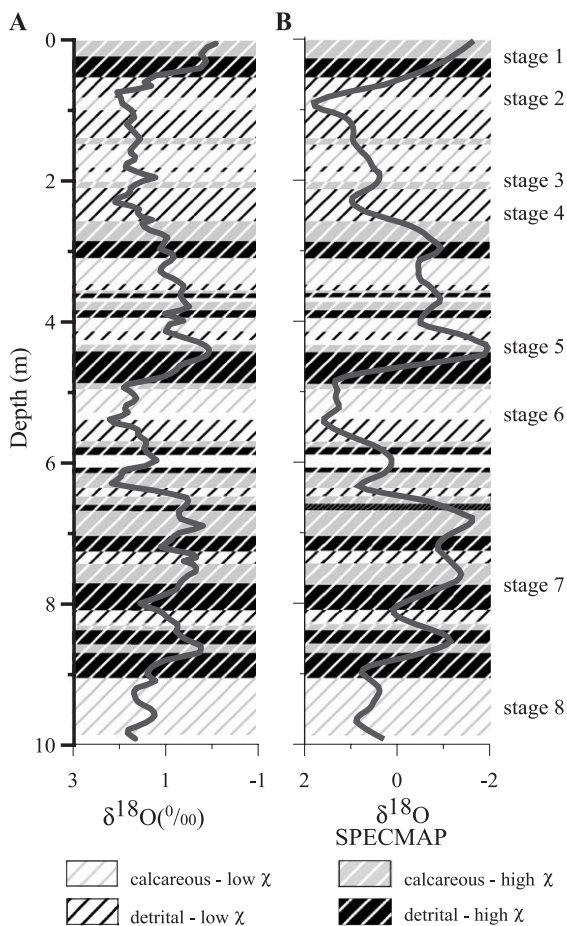


Fig. 14. Assigned clusters compared with (A) the measured $\delta^{18}\text{O}$ data and (B) the $\delta^{18}\text{O}$ stratigraphy based on the SPECMAP curve. Both comparisons indicate that around temperate climate periods the ‘detrital-high χ ’ cluster is always followed by the ‘calcareous-high χ ’ cluster.

10. Climatic interpretation

Univariate analysis of Ba/Al and Ti/Al reveals two major changes in sedimentation related to major climate change: (1) a change in productivity as deduced from Ba/Al and ‘excess Ba’, indicating greater productivity during cold climate periods and (2) a change in detrital input deduced from Ti/Al, indicating a dominant detrital input from the nearby volcanic Azores Islands during temperate climate periods and possibly an increased effect of a second detrital component during glacials. The presence of another detrital input source in cold climate periods is not only suggested by lower Ti/Al ratios but also by the multivariate analyses. (1) Clusters ‘calcareous-high χ ’ and especially ‘detrital-high χ ’ are most similar to volcanic ash layers (Table 2). They are concentrated around temperate climate periods and are hardly found in glacials, suggesting that the detrital volcanic component was less prominent in cold intervals. (2) Prediction of both Mn/Al and Zr/Al by Al with a linear regression model shows a subtle difference between glacials and interglacials. Mn/Al and Zr/Al are generally slightly underestimated during the glacial periods and slightly overestimated during temperate climate periods. These slight differences in lithogenic fractions might be related to a slightly different detrital input as Zr/Al is concerned, but the erratic depth profile of Zr/Al and possible effects of different sources on the normaliser Al in cold and temperate periods prevents us from detecting the sedimentation source.

The two ‘low χ ’ clusters are mainly found in sediments deposited during cold climate periods. χ /Ti and ARM/IRM are slightly higher in these clusters (Table 2), suggesting the presence of more fine grains in sediments deposited during cold climate periods. It is likely that these fine grains are related to detrital changes and not to diagenetic processes, because: (1) the high significance of the multiple regression models between magnetic χ and Al, Ti/Al, and Ba/Al indicates that χ represents a detrital signal with absolute values influenced by dilution and (2) cluster ‘calcareous-low χ ’ and cluster ‘detrital-low χ ’ show these higher ARM/IRM and lower χ /Ti ratios, while samples providing evidence for diagenetic (precipitation) peaks in Fe are only assigned to the ‘calcareous-low χ ’ cluster (Table 2).

Detrital grain size variations are mainly influenced by three factors; source material, wind strength and distance from the source region. Koopmann (1981) studied bulk particle sizes of deposited Saharan dust in the North Atlantic. He found a decreasing particle size with increasing distance from the coast and related small particles (<6 μm) to eolian transport. Extrapolating the data from Koopmann (1981) into the Azores area (no cores were analysed from the vicinity of the Azores Islands) suggests that the contribution of small Saharan dust particles should be in the range 80–90%. This suggests a small particle size (on average) of eolian dust transported to the Azores area. Assuming that a small particle size is accompanied by a fine magnetic grain size, the presence of more fine grains during the cold climate periods may agree with the scenario that the second source of detrital input during the glacials is eolian input of fine Saharan dust. Aridity and stronger winds in the northern Sahara and Iberian Peninsula during these periods (Prospero and Nees, 1977; Sarnthein, 1978) suggest that this mechanism is also most likely on climatological grounds. Lower magnetic concentrations in the glacials support this hypothesis, because Saharan dust is less (ferri)magnetic than volcanic rocks. The heterogeneous signal of the glacial sediments prevents further description of the eolian component (and detection of more detrital components), because with a lack of comparative studies in the region it is difficult to separate local responses from global climate change in such a signal.

In contrast to the glacial intervals, the sedimentary signals around temperate climate periods are remarkably consistent throughout the core. The stratigraphic intervals around the temperate climate periods of stages 7, 5, and 2 are characterised by a peak in Ti/Al followed by a peak in Mn/Al 10 to 15 cm higher in the core. Although less pronounced, the latter peak is accompanied by a higher biogenic component (Fig. 8), as demonstrated by the succession of the ‘detrital-high χ ’ and ‘calcareous-high χ ’ clusters around temperate periods (Fig. 14). The sedimentation source remained probably unchanged during temperate periods because Ti/Al ratios are only slightly lower in cluster ‘calcareous-high χ ’ than in cluster ‘detrital-high χ ’.

With sedimentation rates of around 3.5 cm/ky, the offset between the Ti/Al and Mn/Al peaks corresponds to 3–5.5 ky. This period is too long to attribute the

offset between detrital and biogenic peaks to the recovery of vegetation at the beginning of temperate climate periods (e.g. Rosenbaum et al., 1996). A more plausible explanation for this offset is the sea-level rise at the beginning of the temperate climate periods due to melting of ice-sheets. Morphological observations from Azevedo and Portugal Ferreira (1999) on Flores Island, one of the nine islands of the Azores Archipelago, suggest that relative sea-level was 30–45 m lower during the glacial periods compared to the Holocene and stage 5. As volcanic activity took place on the Azores during all recent glacial periods (Azevedo and Portugal Ferreira, 1999), it is possible that the glacial shores were covered with recent volcanic material from eruptions. This material would have washed into the sea when the sea-level rose at the beginning of temperate climate periods, resulting in a detrital volcanic peak in these sediments. When the ice-sheets shrunk to their interglacial size, sea level rise would have stopped and input from volcanic deposits would have substantially decreased. As a result, the effects of vegetation and soil formation become visible in the sediments by a peak in biogenic input and Mn/Al. The Laurentide and Eurasian continental ice-sheets of the last ice age disappeared about 8 ka B.P., ~4.5 ky after the Late Glacial–Holocene transition (Yu and Wright, 2001), which started at 12.5 ka B.P. Assuming that the duration of the melting of the ice-sheets was similar in previous glacial–interglacial transitions, this mechanism corresponds well with the estimated periods between the Ti/Al and Mn/Al peaks. In this scenario, the biogenic and possibly diagenetic component, as reflected in the ‘calcareous-low χ ’ cluster, is possibly the most typical of climate change. However, this component is initially masked by the detrital volcanic peak and therefore is only visible toward the end of temperate periods.

11. Conclusions

Multivariate statistical analyses show a strong link between magnetic properties and element composition of marine sediments near the Azores Islands. The strong linear correlation between magnetic susceptibility and Al, Ti/Al, and Ba/Al demonstrates that χ is primarily reflects a detrital signal, affected by biogenic dilution. The effects of grain-size variations and

diagenesis on χ are limited. Effects of diagenesis are only visible in Fe/Al peaks between 2 and 4 m depth.

High Ti/Al ratios and magnetic mineral concentrations indicate that detrital input from the nearby Azores Islands is an important sediment source. Lower Ti/Al and χ values and slightly different properties of the lithogenic fraction indicate the presence of at least one other detrital source during glacials. Climatological arguments suggest that eolian deposition of Saharan dust is the most likely second source, but this source cannot be positively identified. Ba/Al ratios can be related to productivity and indicate stronger productivity during glacials.

Cluster analysis shows that sediment properties at the beginning of temperate climate periods are most similar to the properties of the intercalated volcanic ash layers. This peak in detrital volcanic material is followed by a more biogenic and diagenetically influenced peak toward the end of glacial periods. The estimated time lag between both peaks is about 4 ky, which suggests that rising sea-levels would have caused volcanic material deposited on the glacial shores to be washed into the sea at the beginning of the temperate climate periods. Initially, this masked the biogenic component, represented by the ‘calcareous-high χ ’ cluster which may be more typical of environmental changes on the Azores Islands associated with warmer climate. Only after sea-level rise had halted, and deposition of volcanic material decreased, did the biogenic component become visible. This finding warrants further study, because it informs us about the impact of global climate change on a local scale. This study demonstrates that a combined magnetic and chemical approach is powerful for this purpose, because in combination with multivariate statistical analysis it enables detection of subtle changes in sediment properties.

Acknowledgements

We thank Laurent Labeyrie for access to core SU 92-18 and J. Bloemendal and A.P. Roberts for their constructive reviews of earlier versions of the manuscript. This work was supported by the Earth and Life Sciences Division of the Netherlands Organization for Scientific Research (NWO/ALW) and by the Research Institute of the Department of Earth Sciences (Faculty

of Geosciences, Utrecht University). It was conducted under the program of the Vening Meinesz Research School of Geodynamics (VMSG).

References

- Abrantes, F., 2000. 200,000 yr diatom records from Atlantic upwelling sites reveal maximum productivity during LGM and a shift in phytoplankton community structure at 185 000 yr. *Earth Planet. Sci. Lett.* 176, 7–16.
- Aitchinson, J., 1984. The statistical analysis of geochemical compositions. *Math. Geol.* 16, 531–564.
- Azevedo, J.M.M., Portugal Ferreira, M.R., 1999. Volcanic gaps and subaerial records of palaeo-sea-levels on Flores Island (Azores): tectonic and morphological implications. *Geodynamics* 28, 117–129.
- Bezdek, C.J., 1981. *Pattern Recognition with Fuzzy Objective Function Algorithms*. Plenum Press, New York.
- Bond, G., Heinrich, H., Broecker, W., Labeyrie, L., McManus, J., Andrews, J., Huon, S., Jantschik, R., Clasen, S., Simet, C., Tedesco, K., Klas, M., Bonani, G., Ivy, S., 1992. Evidence for massive discharges of icebergs into the North Atlantic Ocean during the last glacial period. *Nature* 360, 245–249.
- Brumsack, H.-J., Gieskes, J.M., 1983. Interstitial water trace-metal chemistry of laminated sediments from the Gulf of California, Mexico. *Mar. Chem.* 14, 89–106.
- Dekkers, M.J., Langereis, C.G., Vriend, S.P., van Santvoort, P.J., de Lange, G.J., 1994. Fuzzy *c*-means cluster analysis of early diagenetic effects on natural remanent magnetization acquisition in a 1.1 Myr piston core from the Central Mediterranean. *Phys. Earth Planet. Inter.* 85, 155–171.
- DeMenocal, P.B., Ruddiman, W.F., Pokras, W.M., 1993. Influences of high- and low-latitude processes on African terrestrial climate: Pleistocene eolian records from equatorial Atlantic Ocean Drilling program site 663. *Paleoceanography* 8, 209–242.
- Dymond, J., Suess, E., Lyle, M., 1992. Barium in deep-sea sediments: a proxy for paleoproductivity. *Paleoceanography* 7, 163–181.
- Hanesch, M., Scholger, R., Dekkers, M.J., 2001. The application of fuzzy *c*-means cluster analysis and non-linear mapping to a soil data set for the detection of polluted sites. *Phys. Chem. Earth, Part A Solid Earth Geod.* 26, 885–891.
- Hinrichs, J., Schnetger, B., Schale, H., Brumsack, H.-J., 2001. A high-resolution study of NE Atlantic sediments at station Bengal: geochemistry and early diagenesis of Heinrich layers. *Mar. Geol.* 177, 79–92.
- Huber, P., 1981. *Robust Statistics*. Wiley, New York.
- Jackson, M., 1991. Anisotropy of magnetic remanence: a brief review of mineralogical sources, physical origins, geological applications, and comparison with susceptibility anisotropy. *Pure Appl. Geophys.* 136, 1–28.
- Kolla, V., Biscaye, P., Hanley, A.F., 1979. Distribution of quartz in late Quaternary Atlantic sediments in relation to climate. *Quat. Res.* 11, 261–277.
- Koopmann, B., 1981. Sedimentation von Saharastaub im subtropischen Nordatlantik während der letzten 25.000 Jahre. *Meteor. Forsch. Ergeb.* 35, 23–59.
- Kruiver, P.P., Kok, Y.S., Dekkers, M.J., Langereis, C.G., Laj, C., 1999. A pseudo-Thellier relative palaeointensity record, and rock magnetic and geochemical parameters in relation to climate during the last 276 kyr in the Azores region. *Geophys. J. Int.* 136, 757–770.
- Kruiver, P.P., Dekkers, M.J., Heslop, D., 2001. Quantification of magnetic coercivity components by the analysis of acquisition curves of isothermal remanent magnetisation. *Earth Planet. Sci. Lett.* 189, 269–276.
- Lacasse, C., Paterne, M., Werner, R., Wallrabe-Adams, H.-J., Sigurdsson, G., Carey, S., Pinte, G., 1996. Geochemistry and origin of Pliocene and Pleistocene ash layers from the Icelandic Plateau, Site 907, Leg 151. In: Myhre, A., et al., (Eds.), *Arctic Gateways. Proc. ODP, Sci. Res.*, pp. 310–331.
- Lackschewitz, K.S., Wallrabe-Adams, H.-J., 1997. Deposition and origin of volcanic ash zones in Late Quaternary sediments from the Reykjanes Ridge: evidence for ash fallout and ice-rafting. *Mar. Geol.* 136, 209–244.
- Larrasoana, J.C., Roberts, A.P., Stoner, J.S., Richter, C., Wehausen, R., 2003a. A new proxy for bottom-water ventilation in the eastern Mediterranean based on diagenetically controlled magnetic properties of sapropel-bearing sediments. *Palaeogeogr. Palaeoclimatol. Palaeoecol.* 190, 221–242.
- Larrasoana, J.C., Roberts, A.P., Rohling, E.J., Winkhofer, M., Wehausen, R., 2003b. Three million year of monsoon variability over the northern Sahara. *Clim. Dyn.* 21, 689–698.
- Lehman, B., Laj, C., Bard, E., Arnold, M., Tric, E., 1997. Relative changes of the geomagnetic field intensity during the last 280 kyear from piston cores in the Azores area. *Phys. Earth Planet. Int.* 114, 39–57.
- Liotard, J.M., Barszczus, H.G., Dupuy, D., Dostal, J., 1986. Geochemistry and origin of basaltic lavas from Marquesas Archipelago, French Polynesia. *Contrib. Mineral. Petrol.* 92, 260–268.
- Lourens, L.J., Wehausen, R., Brumsack, H.-J., 2001. Geological constraints on tidal dissipation and dynamical ellipticity of the Earth over the past three million years. *Nature* 409, 1029–1033.
- Luckge, A., Dooze-Rolinski, H., Khan, A.A., Schulz, H., von Rad, U., 2001. Monsoon variability in the northeastern Arabian Sea during the past 5000 years: geochemical evidence from laminated sediments. *Palaeogeogr. Palaeoclimatol. Palaeoecol.* 167, 273–286.
- Mahowald, N., Kohfeld, K., Hansson, M., Balkanski, Y., Harrison, S.P., Prentice, I.C., Schulz, M., Rodhe, H., 1999. Dust sources and deposition during the last glacial maximum and current climate: a comparison of model results with paleodata from ice cores and marine sediments. *J. Geophys. Res.* 104, 15895–15916.
- Martinson, D.G., Pisias, N.G., Hays, J.D., Imbrie, J., Moore, T.C., Shackleton, N.J., 1987. Timing and the orbital theory of the ice ages: development of a high resolution 0–300,000 years stratigraphy. *Quat. Res.* 27, 1–29.
- McManus, J., Berelson, W.M., Klinkhammer, G.P., Johnson, K.S., Coale, K.H., Anderson, R.F., Klumar, N., Burdige, D.J.,

- Hammond, D.E., Brumsack, H.J., McCorkle, D.C., Rushdi, A., 1998. Geochemistry of barium in marine sediments: implications for its use as a paleoproxy. *Geochim. Cosmochim. Acta* 62, 3453–3473.
- Moreno, A., Taragona, J., Henderiks, J., Canals, M., Freudenthal, T., Meggers, H., 2001. Orbital forcing of dust supply to the North Canary Basin over the last 250 kyr. *Quat. Sci. Rev.* 20, 1317–1339.
- Paillier, D., Bard, E., 2002. High frequency palaeoceanographic changes during the past 140,000 yr recorded by the organic matter in sediments of the Iberian Margin. *Palaeogeogr. Palaeoclimatol. Palaeoecol.* 181, 431–452.
- Prospero, J.M., Nees, R.T., 1977. Dust concentration in the atmosphere of the equatorial North Atlantic: possible relationship to Sahelian drought. *Science* 196, 1196–1198.
- Rea, D.K., 1994. The paleoclimatic record provided by eolian deposition in the deep sea: the geologic history of wind. *Rev. Geophys.* 32, 159–195.
- Robinson, S.G., Sahota, J.T.S., Oldfield, F., 2000. Early diagenesis in North Atlantic abyssal plain sediments characterized by rock-magnetic and geochemical indices. *Mar. Geol.* 163, 77–107.
- Rosenbaum, J.G., Reynolds, R.L., Adam, D.P., Drexler, J., Sarna-Wojcicki, A., Whitney, G.C., 1996. Record of middle Pleistocene climate change from Buck Lake, Cascade Range, southern Oregon—Evidence from sediment magnetism, trace element geochemistry, and pollen. *Bull. Geol. Soc. Am.* 108, 1328–1341.
- Sarnthein, M., 1978. Sand deserts during glacial maximum and climatic optimum. *Nature* 272, 43–45.
- Sarnthein, M., Winn, K., Duplessy, J.C., Fontugue, M.R., 1988. Global variations of surface ocean productivity. *Paleoceanography* 3, 381–399.
- Schmidt, A.M., von Dobeneck, T., Bleil, U., 1999. Magnetic characterisation of Holocene sedimentation in the South Atlantic. *Paleoceanography* 14, 465–481.
- Tauxe, L., Mullender, T.A.T., Pick, T., 1996. Potbellies, wasp-waists and superparamagnetism in magnetic hysteresis. *J. Geophys. Res.* 101, 571–583.
- Thomson, J., Higgs, N.C., Jarvis, I., Hydes, D.J., Colley, S., Wilson, R.T.S., 1986. The behaviour of manganese in Atlantic carbonate sediments. *Geochim. Cosmochim. Acta* 50, 1807–1818.
- Tiedemann, R., Sarnthein, M., Shackleton, N.J., 1994. Astronomic timescale for Pliocene Atlantic $\delta^{18}\text{O}$ and dust flux records of Ocean Drilling Program site 659. *Paleoceanography* 9, 619–638.
- Urbat, M., Dekkers, M.J., Vriend, S.P., 1999. The isolation of diagenetic groups in marine sediments using fuzzy c-means cluster analysis, in *Paleomagnetism and Diagenesis in Sediments*. In: Tarling, D.H., Turner, P. (Eds.), *Paleomagnetism and Diagenesis in Sediments*, Spec. Publ.—Geol. Soc., Lond., vol. 151, pp. 85–93.
- Versteegh, G.J.J., Brinkhuis, H., Visscher, H., Zonneveld, K.A.F., 1996. The relation between productivity and temperature in the Pliocene North Atlantic at the onset of northern hemisphere glaciation: a palynological study. *Glob. Planet. Change* 11, 155–165.
- Vigliotti, L., Capotondi, L., Torii, M., 1999. Magnetic properties of sediments deposited in suboxic-anoxic environments: relationships with biological and geochemical parameters. In: Tarling, D.H., Turner, P. (Eds.), *Paleomagnetism and Diagenesis in Sediments*. Spec. Publ.—Geol. Soc., Lond., vol. 151, pp. 71–83.
- Vlag, P., Hoepfner, S., Martinus, G., Renssen, R., 2000. Application of robust statistics to practical problems. *Proc. of Comp. Statistics*, B, pp. 19–22.
- von Breymann, M.T., Emeis, K.-C., Suess, E., 1992. Water depth and diagenetic constraints on the use of barium as a palaeoproductivity indicator. In: Summerhayes, C.P., Prell, E.L., Emeis, K.-C. (Eds.), *Upwelling Systems: Evolution since the Early Miocene*. Special Publication—Geological Society, vol. 64, pp. 131–145.
- Vriend, S.P., van Gaans, P.F., Middelburg, J., de Nijs, A., 1988. The application of fuzzy c-means cluster analysis and non-linear mapping to geochemical data sets: examples from Portugal. *Appl. Geochem.* 3, 213–224.
- Wehausen, R., Brumsack, H.-J., 1999. Cyclic variations in the chemical composition of eastern Mediterranean Pliocene sediments: a key for understanding sapropel formation. *Mar. Geol.* 153, 161–176.
- Wehausen, R., Brumsack, H.-J., 2000. Chemical cycles in Pliocene sapropel-bearing and sapropel-barren eastern Mediterranean sediments. *Palaeogeogr. Palaeoclimatol. Palaeoecol.* 158, 325–352.
- Yu, Z., Wright Jr., H.E., 2001. Response of interior North America to abrupt climate oscillations in the North Atlantic region during the last deglaciation. *Earth-Sci. Rev.* 52, 333–369.